Monitoring the Birth of an Electronic Wavepacket in a Neutral Molecule with Attosecond Time-Resolved Photoelectron Spectroscopy

ARTICLE *in* THE JOURNAL OF PHYSICAL CHEMISTRY A · JUNE 2014

Impact Factor: 2.69 · DOI: 10.1021/jp508218n · Source: arXiv

6 AUTHORS, INCLUDING:

Aurelie Perveaux
Institut Charles Gerhardt - Laboratoire de chi…
8 PUBLICATIONS **21** CITATIONS
SEE PROFILE

Fabien Gatti
Institut Charles Gerhardt
137 PUBLICATIONS **2,168** CITATIONS
SEE PROFILE

Ágnes vibók
University of Debrecen
103 PUBLICATIONS **1,117** CITATIONS
SEE PROFILE

THE JOURNAL OF PHYSICAL CHEMISTRY A

Article

pubs.acs.org/JPCA

Monitoring the Birth of an Electronic Wavepacket in a Molecule with Attosecond Time-Resolved Photoelectron Spectroscopy

Aurelie Perveaux,[†,‡] David Lauvergnat,[‡] Fabien Gatti,[†] Gábor J. Halász,[§] Ágnes Vibók,*[,∥] and Benjamin Lasorne[†]

[†]Institut Charles Gerhardt, CNRS, Université Montpellier 2, F-34095 Montpellier, France

[‡]Laboratoire de Chimie Physique, CNRS, Université Paris-Sud, F-91405 Orsay, France

[§]Department of Information Technology, University of Debrecen, H-4010 Debrecen, P.O. Box 12, Hungary

[∥]Department of Theoretical Physics, University of Debrecen, H-4010 Debrecen, P.O. Box 5, Hungary

ABSTRACT: Numerical simulations are presented to validate the possible use of cutting-edge attosecond time-resolved photoelectron spectroscopy to observe in real time the creation of an electronic wavepacket and subsequent electronic motion in a neutral molecule photoexcited by a UV pump pulse within a few femtoseconds.

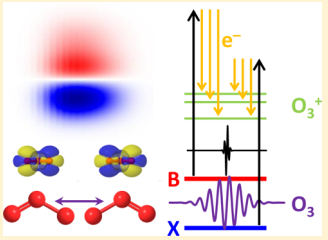

The recent emergence of attosecond extreme-ultraviolet (XUV) pulses[1,2] has given access to observing and controlling ultrafast electronic motions in real time.[3−9] Goulielmakis and co-workers provided the first images of electronic motion in atoms using an attosecond probe pulse.[7] Such techniques have thus opened the door to studying molecular processes such as ultrafast charge migration after sudden ionization[10,11] and ultrafast exciton migration after creating a coherent superposition of electronic states.[12−15] Experimentally, laser control on the subfemtosecond time scale has already been evidenced for diatomic molecules: in the dissociative ionization of the D_2 and CO molecules using the carrier envelope phase of a few-cycle pulse[16,17] to induce charge localization in the molecular cation; with the direct manipulation of charge oscillations in K_2[18,19] using selective population of dressed states within the framework of strong-field temporal control.

Attochemistry, i.e., laser control based on electronic coherence in a neutral molecule, should soon become a realistic technique, whereby the electronic motion is steered before the nuclear motion can occur and thus before intramolecular vibrational relaxation can play a role. In other words, one should now expect to possess the experimental tools for observing how chemical bonds really move in a molecular system over the course of a reaction and further control bond breaking and formation in real time. Ultrashort sources of coherent light are now approaching the few-femtosecond regime for UV laser pulses, whereas attosecond pulses are already available in the XUV domain. One can also expect the emergence of few-cycle UV subfemtosecond pulses in a near future. However, deciphering experimental results in this context may prove challenging unless they are supported by an interpretation based on relevant numerical simulations and adequate theoretical representations.

Ozone is a well-studied small triatomic molecule that can be handled theoretically with high precision, and many theoretical and experimental data such as, e.g., photoelectron spectra or absorption cross sections are available for it. This molecule, of critical relevance for atmospheric physics and chemistry, exhibits a high absorption cross section between 200 and 300 nm followed by dissociation. This process explains the protective role of the ozone layer in the Earth's atmosphere with respect to UV light from the Sun. From the experimental point of view, this also implies that ozone can be efficiently excited electronically by means of few-cycle third harmonic pulses of Ti:Sa lasers. In this UV region (called the Hartley band), the absorption is mostly due to a single electronic excited state (denoted B), such that an ultrashort UV pulse is expected to create a superposition of the electronic ground state (X) and the B state almost exclusively, thus making ozone a good candidate for observing a well-defined electronic wavepacket made of two states.

In previous works, we described with accurate quantum dynamics simulations the coupled electronic and nuclear motion in ozone after photoexcitation by a 3 fs UV pump pulse.[20,21,24] An initial molecular wavepacket was prepared as a coherent superposition of the X and B states (see Figure 1 for the potential energies along the dissociation coordinate) whereby neither the electrons nor the nuclei were in a stationary state. The multiconfiguration time-dependent Hartree (MCTDH) method[22,23] was applied to solve the time-dependent nuclear Schrödinger equation within a two-

Received: August 13, 2014
Revised: August 27, 2014

   dx.doi.org/10.1021/jp508218n | J. Phys. Chem. A XXXX, XXX, XXX−XXX

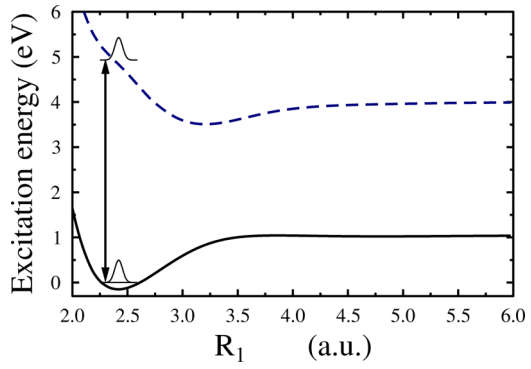

Figure 1. Potential energy surfaces of ozone as functions of the dissociation coordinate, R_1: ground state (X, solid line) and Hartley state (B, dashed line). The arrow denotes excitation of the B state. The other bond is fixed at R_2= 2.43 au and the bond angle is θ = 117°.

electronic-state coupled representation. The details and the analysis of the calculations can be found in refs.[20,21,24]

We examined the time evolution of the electron density at the Franck−Condon (FC) point. This picture is representative of the electronic motion on the ultrashort time scale, as long as the nuclei do not move significantly (that is, during the first 5−6 fs), which is precisely the focus of the present work. The resulting electron density showed a periodic transfer between the two chemical bonds, which could be interpreted in chemical terms as an ultrafast oscillation between both mesomers of ozone (the two equivalent Lewis structures with localized charges and single or double bonds on either one or the other side of the molecule).

The objective of the present work is to establish a more realistic connection with potential experiments that could monitor in real time the creation of an electronic wavepacket in a neutral molecule after photoexcitation by an ultrashort UV pulse. In this, the pump should be no longer than a few femtoseconds (not to trigger the nuclear motion), whereas the probe should be even shorter to observe the electronic motion with high-enough time resolution. The method of choice would thus be time-resolved photoelectron spectroscopy[25−31] using an attosecond XUV probe pulse. However, such experiments may not provide clear-cut evidence for different reasons. Many ionic channels can be accessed upon photoionizing from either X or B, and a number of transitions will overlap within the same energy window. In addition, the bandwidth of the attosecond probe will be large: a few electronvolts for a few-hundred-attoseconds pulse. This may prevent any characteristic feature in the spectrum to be observed. Preliminary numerical simulations are thus required to prove first that contributions from X or B can be discriminated over time and to identify which energy window is adequate. To this end, we generated an approximate time-resolved photoelectron spectrum (TRPES) based on accurate quantum dynamics and quantum chemistry calculations, as further explained below. Our results show that the depletion of X and the production of B will appear in distinct energy regions, despite a large bandwidth and overlapping channels.

Let us start with the photoelectron spectra obtained by photoionizing either X or B. First, assuming an "atomic" picture (whereby the rovibrational dynamics and its influence on the structure of the spectrum are ignored), the energy resolved photoelectron spectra for k = X, B appear as stick spectra (Figure 2a),

$$I_k(\varepsilon) = \sum_j I_{jk}\delta(\varepsilon - \varepsilon_{jk}) \tag{1}$$

where ε is the kinetic energy release (KER) of the electron, with lines centered at

$$\varepsilon_{jk} = E_k + E_{\text{photon}} - E_j \tag{2}$$

using a probe energy E_{photon} = 95 eV. Here E_k and E_j are the energies of the neutral molecule in the ground or excited state, X or B, and of the cation in the ground or one of the excited states among the first 18, respectively, up to about 20 eV above X (Table 1). $I_{jk} = \langle \Phi_{j,k}^{\text{Dyson}} | \Phi_{j,k}^{\text{Dyson}} \rangle$ are the Dyson norms calculated at the FC point where the Dyson orbitals are defined as

$$\Phi_{j,k}^{\text{Dyson}}(\vec{r};\vec{R}) = \sqrt{N} \int \mathrm{d}\vec{r}_1 \ldots \mathrm{d}\vec{r}_{N-1} \psi_{\text{el,neut}}^{N,k}(\vec{r}_1,\ldots\vec{r}_N=\vec{r};\vec{R})\, \psi_{\text{el,cat}}^{N-1,j}(\vec{r}_1,\ldots\vec{r}_{N-1};\vec{R}) \tag{3}$$

The corresponding electronic structure calculations were performed with the MOLPRO package[36] at the MRCI/aug-cc-pVQZ level of theory.[37]

Assuming one-photon XUV ionization and using the sudden approximation[33] the Dyson norms at the FC point (see their values in Table 2 for the present situation) are expected to be near proportional to the relative ionization probabilities.[31] The proportionality factor can be considered as constant when the continuum does not exhibit a rich structure. In this treatment the Dyson norms are a measure of the relative intensities of the corresponding peaks (Figure 2a).

The first three states of the cation correspond to intense and narrow peaks in the photoelectron spectrum when ionizing from X[32] (ionization potentials around 12−13 eV), thus

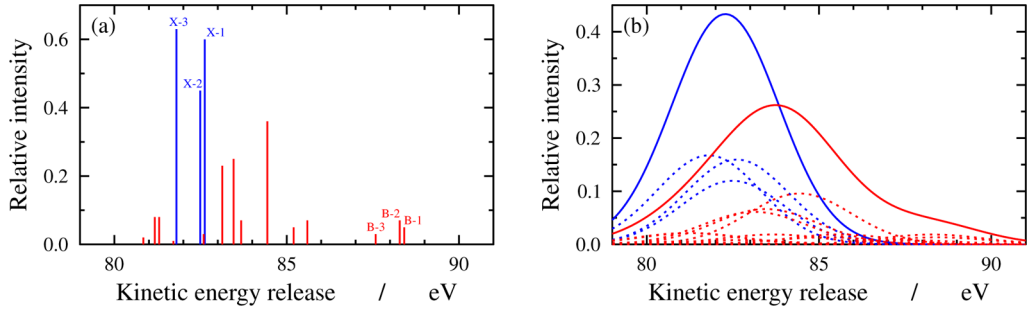

Figure 2. (a) Stick photoelectron spectra from X (blue) or B (red) as functions of the kinetic energy release for a probe photon at 95 eV. (b) Convoluted photoelectron spectra from X (blue) or B (red) as functions the kinetic energy release (KER) for a probe photon at 95 eV.

dx.doi.org/10.1021/jp508218n | J. Phys. Chem. A XXXX, XXX, XXX−XXX

Table 1. *Ab initio* Ionization Potentials (MRCI/cc-pVQZ Level of Theory) with Respect to Either X or B at the FC Point[a]

cation states (j)	$E_j - E_X$/eV	$E_j - E_B$/eV
$1(1^2A_1)$	12.38	6.59
$2(1^2B_2)$	12.51	6.72
$3(1^2A_2)$	13.20	7.42
$4(1^2B_1)$	14.15	8.36
$5(2^2A_2)$	14.45	8.66
$6(2^2B_2)$	15.18	9.40
$7(2^2A_1)$	15.58	9.80
$8(2^2B_1)$	16.35	10.56
$9(3^2A_2)$	16.50	10.72
$10(3^2B_1)$	17.10	11.32
$11(3^2A_1)$	17.32	11.54
$12(3^2B_2)$	17.65	11.87
$13(4^2B_2)$	18.19	12.41
$14(4^2A_2)$	18.63	12.85
$15(4^2B_1)$	18.61	12.83
$16(4^2A_1)$	19.07	13.29
$17(5^2B_2)$	19.61	13.83
$18(5^2A_1)$	19.49	13.70
$19(6^2B_2)$	19.94	14.16

[a]The energy difference between the X and the B states is 5.78 eV. See ref 32 for a comparison with computed and experimental values.

Table 2. Dyson Norms at the FC Point

state pairs	Dyson norms	state pairs	Dyson norms
neutral X-cation 1	0.60	neutral B-cation 1	0.05
neutral X-cation 2	0.45	neutral B-cation 2	0.07
neutral X-cation 3	0.63	neutral B-cation 3	0.03
neutral X-cation 4	0.00	neutral B-cation 4	0.00
neutral X-cation 5	0.00	neutral B-cation 5	0.00
neutral X-cation 6	0.01	neutral B-cation 6	0.07
neutral X-cation 7	0.00	neutral B-cation 7	0.05
neutral X-cation 8	0.19	neutral B-cation 8	0.36
neutral X-cation 9	0.00	neutral B-cation 9	0.00
neutral X-cation 10	0.08	neutral B-cation 10	0.07
neutral X-cation 11	0.20	neutral B-cation 11	0.25
neutral X-cation 12	0.04	neutral B-cation 12	0.23
neutral X-cation 13	0.01	neutral B-cation 13	0.03
neutral X-cation 14	0.00	neutral B-cation 14	0.00
neutral X-cation 15	0.00	neutral B-cation 15	0.00
neutral X-cation 16	0.00	neutral B-cation 16	0.01
neutral X-cation 17	0.03	neutral B-cation 17	0.08
neutral X-cation 18	0.22	neutral B-cation 18	0.08
neutral X-cation 19	0.19	neutral B-cation 19	0.02

making them good candidates for characterizing the time evolution of the population of X. If ionization also occurs from B, and accounting for an energy shift between both states of about 6 eV, means that these three peaks may overlap with peaks corresponding to ionization potentials from X around 18−19 eV (between B-12 and B-16; Tables 1 and 2). We thus limited the KER window to a lower bound of 80.8 eV for a probe photon at 95.0 eV, thus restricting j to 1, ..., 4 when ionizing from X and to 1, ..., 19 from B, according to the energies given in Table 1. As can be observed in Figure 2a, both spectra from X and B appear together below 83 eV (but the peaks from X dominate), whereas only B contributes above 83 eV with peaks of significant magnitude.

Now, such a clear discrimination between both types of spectra could be lost once accounting for the widths of the peaks. An intrinsic width will be due to the rovibrational structure for each photoionization, whereas the bandwidth of the probe pulse may further enlarge them. We used a probe pulse of full duration at half-maximum (FDHM) of 500 as, corresponding to a standard deviation of the intensity $\sigma = 1.5$ eV in the energy domain. In this context, the broadening of the spectra due to the bandwidth is far larger than that due to the rovibrational structure, thus validating an "atomic" picture as a first approximation (fixing the geometry at the FC point for determining the relative intensities of the peaks). We thus convoluted the stick spectra with a Gaussian window function of standard deviation σ, so as to mimic the bandwidth of the XUV photoionizing probe pulse,

$$I_k(\varepsilon) = \frac{1}{\sigma\sqrt{2\pi}} \sum_j \mathrm{e}^{-(\varepsilon-\varepsilon_{jk})^2/2\sigma^2} I_{jk} \tag{4}$$

The resulting energy-resolved spectra are shown on Figure 2b. Despite the strong enlargment, it is to be expected that contributions from X and B can be discriminated below and above 83 eV, respectively.

Now, to simulate the creation of a coherent superposition of X and B, we performed quantum dynamics simulations in the presence of a UV linearly polarized Gaussian laser pump pulse with a carrier wavelength and intensity at 260 nm and 10^{13} W/cm^2, respectively. The FDHM (full-duration half-maximum) was 3 fs. The PESs and $\vec{R}$-dependent dipole moments occurring in the radiative coupling terms were taken from refs 34 and 35. The FC point ($R_1 = R_2 = 1.275$ Å; $\theta = 116.9°$) of the ozone molecule has C_{2v} symmetry and therefore only the y-component (B_2) of the transition dipole between X ($^1A_1$) and B ($^1B_2$) is nonzero. Thus, the only effective polarization of the electric field is y.

The resulting molecular wavepacket is expanded as

$$|\psi_{\mathrm{mol}}(\vec{R},t)\rangle = \sum_{k=\mathrm{X,B}} \psi_{\mathrm{nuc}}^{(k)}(\vec{R},\, t)|\psi_{\mathrm{el}}^{(k)};\vec{R}\rangle \tag{5}$$

Again, using an "atomic" picture at the FC point, we define an effective electronic wavepacket as ($\vec{R} = \vec{R}_{\mathrm{FC}}$),

$$|\psi_{\mathrm{el}}(t)\rangle = \sum_{k=\mathrm{X,B}} c_k(t)|\psi_{\mathrm{el}}^{(k)};\vec{R}_{FC}\rangle \tag{6}$$

where $|\psi_{\mathrm{el}}^{(k)};\vec{R}_{\mathrm{FC}}\rangle$ are the adiabatic electronic states of the neutral molecule at the FC point and $c_k(t)$ are the renormalized nuclear wave packet components,

$$c_k(t) = \frac{\psi_{\mathrm{nuc}}^{(k)}(\vec{R}_{\mathrm{FC}},t)}{\sqrt{\sum_{l=\mathrm{X,B}} |\psi_{\mathrm{nuc}}^{(l)}(\vec{R}_{\mathrm{FC}},t)|^2}} \tag{7}$$

The corresponding local populations ($k = k'$) and coherences ($k \neq k'$) at the FC point are (Figure 3)

$$\rho_{kk'}(t) = c_k^*(t)\, c_{k'}(t) = \frac{\psi_{\mathrm{nuc}}^{(k)*}(\vec{R}_{\mathrm{FC}},t)\, \psi_{\mathrm{nuc}}^{(k')}(\vec{R}_{\mathrm{FC}},t)}{\sum_{l=\mathrm{X,B}} |\psi_{\mathrm{nuc}}^{(l)}(\vec{R}_{\mathrm{FC}},\, t)|^2} \tag{8}$$

As expected, the local populations and coherences are similar to the global ones up to about 3 fs, which is the focus of the present work. They further decay while the nuclear wavepackets escape the FC region, whereas the global populations stay constant. The Dyson norms actually depend on the

dx.doi.org/10.1021/jp508218n | J. Phys. Chem. A XXXX, XXX, XXX−XXX

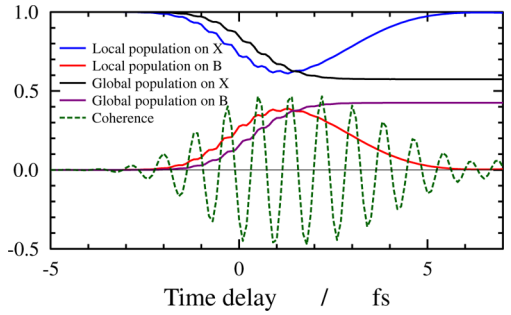

Figure 3. Local X (blue) and B (red) populations and coherence (green; real part) at the FC point as functions of time (origin coincident with the maximum of the pump pulse). Global X (black) and B (purple) populations ($P_k(t) = \int \rho_{kk}(\vec{R},\vec{R},t)\, d\vec{R}$) as functions of time).

molecular geometry. This should be accounted for and correctly integrated over the nuclear coordinates when the TRPES is estimated for longer times. The limiting case used here would keep its validity if the Dyson norms had significant magnitudes in the FC region and decreased quickly when the molecule dissociates. One would thus observe directly the escape of the wavepacket in the decay of the TRPES signal. On the other hand, the other limiting case with homogeneous Dyson norms would yield a constant signal beyond 3 fs. The experimental signal is likely to be somewhere in between.

In any case, monitoring the photoelectron spectrum of such a coherent superposition of X and B as a function of the time delay, τ (between the maximum of the probe and the maximum of the pump), is expected to yield a time-dependent pattern that should reflect depletion of X below 83 eV and production of B above 83 eV on the ultrashort time scale. For a stick spectrum, the intensity as a function of the time delay can be approximated as (for each cation channel):

$$I_j(\tau) = \sum_{k=\mathrm{X,B}} \rho_{kk}(\tau) I_{jk} \tag{9}$$

Using the same convolution procedure as above leads to the following expression for the TRPES (Figure 4),

$$I(\varepsilon,\tau) = \sum_{k=\mathrm{X,B}} \rho_{kk}(\tau)\, I_k(\varepsilon) = \frac{1}{\sigma\sqrt{2\pi}} \sum_{k=\mathrm{X,B}} \rho_{kk}(\tau) \sum_j \mathrm{e}^{-(\varepsilon-\varepsilon_{jk})^2/2\sigma^2} I_{jk} \tag{10}$$

Two significant effects can be noticed on Figure 4: (i) around 82 eV (panel b), between τ = 0 and 3 fs—while the pump pulse is still on—the intensity decreases to 0.33, in contrast with its value of 0.40 for τ < 0 or >3 fs; (ii) around 86 eV (panel c) the intensity increases from 0.01 to 0.04 and returns to 0.01 during the same delay time intervals. Better contrast is obtained by considering the differential TRPES obtained by removing the contribution from pure X at all times (Figure 5) in a similar

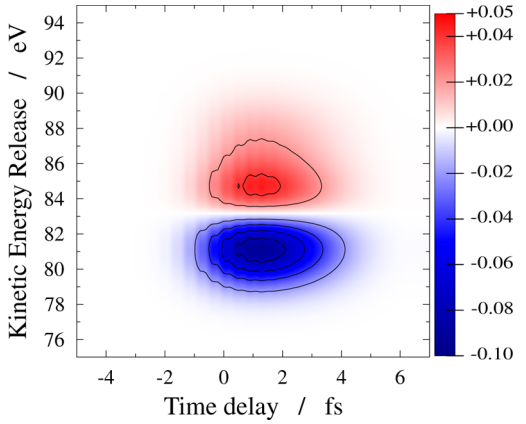

Figure 5. Approximate differential TRPES as a function of the time delay (horizontal axis) and kinetic energy release (vertical axis).

fashion to differential optical densities in transient absorption spectroscopy. The depletion of X and the concommitent production of B are clearly characterized. Again, results up to 3 fs are expected to be similar to experiments, whereas the behavior beyond this time will depend on how the photoionization probability depends on the molecular geometry. Our focus here is the ultrashort time scale in the context of attophysics and the emerging attochemistry field, whereby sterring directly the electrons of a molecule is expected to provide control over reaction mechanisms in a near future.

The central objective of this theoretical work was to determine with numerical simulations if TRPES experiments will be able to monitor the generation of an electronic

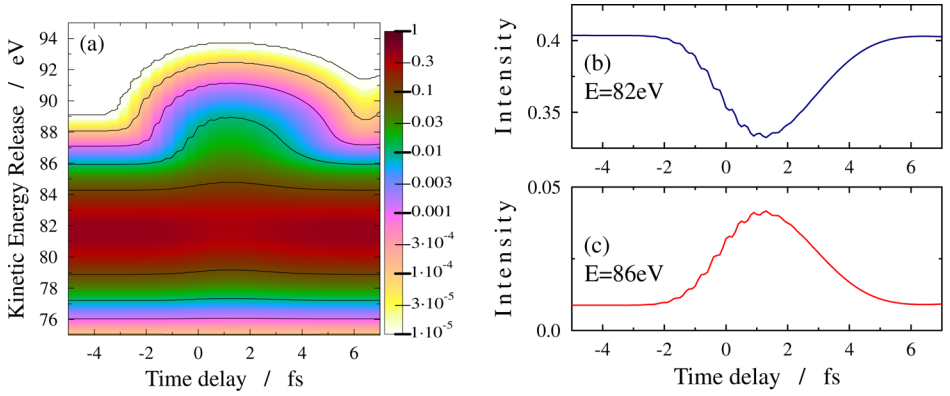

Figure 4. (a) Approximate TRPES (logarithmic scale) as a function of the time delay (horizontal axis) and kinetic energy release (vertical axis). (b) Cut at 82 eV (linear scale). (c) Cut at 86 eV (linear scale).

dx.doi.org/10.1021/jp508218n | J. Phys. Chem. A XXXX, XXX, XXX−XXX

wavepacket in the ozone molecule on its real time scale. Observing the electronic motion in the neutral before any significant nuclear motion requires using a few-femtosecond UV pulse as a pump. Getting high-enough time resolution implies using an XUV attosecond pulse as a probe. The main limitation of such a measurement is the poor energy resolution due to the large bandwidth of the photoionizing pulse. However, we have shown that two energy regions can be distinguished: one exhibiting depletion of X and one where production of B is specifically observed. Such conclusions await further confirmation from experimental investigations.

AUTHOR INFORMATION

Corresponding Author

*E-mail: vibok@phys.unideb.hu.

Notes

The authors declare no competing financial interest.

ACKNOWLEDGMENTS

The authors thank F. Krausz, R. Kienberger, and M. Jobst for support and for fruitful discussions. We acknowledge R. Schinke for providing the diabatic potential energy surfaces and the transition dipole moments and H.-D. Meyer for fruitful discussions. Á.V. also acknowledges the TÁMOP-4.2.4.A/2-11/1-2012-0001 "National Excellence Program" and the OTKA (NN103251) project. Financial support by the CNRS-MTA is gratefully acknowledged.

REFERENCES

(1) Corkum, P.; Krausz, F. Attosecond Science. *Nat. Phys.* **2007**, *3*, 381−387.

(2) Krausz, F.; Ivanov, M. Attosecond Physics. *Rev. Mod. Phys.* **2009**, *81*, 163−234.

(3) Smirnova, O.; Mairesse, Y.; Patchkovskii, S.; Dudovich, N.; Villeneuve, D.; Corkum, P.; Ivanov, M. Y. High Harmonic Interferometry of Multi-Electron Dynamics in Molecules. *Nature* **2009**, *460*, 972−977.

(4) Zhou, X.; Ranitovic, P.; Hogle, C. W.; Eland, J. H. D.; Kapteyn, H. C.; Murnane, M. M. Probing and Controlling non-Born−Oppenheimer Dynamics in Highly Excited Molecular Ions. *Nat. Phys.* **2012**, *8*, 232−237.

(5) Rohringer, N.; Gordon, A.; Santra, R. Configuration-Interaction-Based Time-Dependent Orbital Approach for *ab initio* Treatment of Electronic Dynamics in a Strong Optical Laser Field. *Phys. Rev. A* **2006**, *74*, 043420-1−9.

(6) Rohringer, N.; Santra, R. Multichannel Coherence in Strong-Field Ionization. *Phys. Rev. A* **2009**, *79*, 053402-1−10.

(7) Goulielmakis, E.; et al. Real-Time Observation of Valence Electron Motion. *Nature Lett.* **2010**, *466*, 739−743.

(8) Dixit, G.; Vendrell, O.; Santra, R. Imaging Electronic Quantum Motion with Light. *Proc. Natl. Acad. Sci. U. S. A.* **2012**, *109*, 11636−11640.

(9) Neidel, C.; et al. Probing Time-Dependent Molecular Dipoles on the Attosecond Time Scale. *Phys. Rev. Lett.* **2013**, *111*, 033001-1−5.

(10) Kuleff, A. I.; Breidbach, J.; Cederbaum, L. S. Multielectron Wave-Packet Propagation: General Theory and Application. *J. Chem. Phys.* **2005**, *123*, 044111-1−10.

(11) Remacle, F.; Levine, R. D. Attosecond Pumping of Nonstationary Electronic States of LiH: Charge Shake-Up and Electron Density Distortion. *Phys. Rev. A* **2011**, *83*, 013411-1−8.

(12) Bandrauk, A. D.; Chelkowski, S.; Corkum, P. B.; Manz, J.; Yudin, G. L. Attosecond Photoionization of a Coherent Superposition of Bound And Dissociative Molecular States: Effect of Nuclear Motion. *J. Phys. B* **2009**, *42*, 134001−7.

(13) Grafe, S.; Engel, V.; Ivanov, M. Y. Attosecond Photoelectron Spectroscopy of Electron Tunneling in a Dissociating Hydrogen Molecular Ion. *Phys. Rev. Lett.* **2008**, *101*, 103001-1−4.

(14) Geppert, D.; von den Hoff, P.; de Vivie-Riedle, R. Electron Dynamics In Molecules: A New Combination of Nuclear Quantum Dynamics and Electronic Structure Theory. *J. Phys. B* **2008**, *41*, 074006-1−8.

(15) Mignolet, B.; Levine, R. D.; Remacle, F. Localized Electron Dynamics In Attosecond-Pulse-Excited Molecular Systems: Probing the Time-dependent Electron Density by Sudden Photoionization. *Phys. Rev. A* **2012**, *86*, 053429-1−8.

(16) Kling, M. F.; Siedschlag, Ch.; Verhoef, A. J.; Khan, J. I.; Schultze, M.; Uphues, Th.; Ni, Y.; Uiberacker, M.; Drescher, M.; Krausz, F.; et al. Control of Electron Localization in Molecular Dissociation. *Science* **2006**, *312*, 246−248.

(17) Znakovskaya, I.; von den Hoff, P.; Zherebtsov, S.; Wirth, A.; Herrwerth, O.; Vrakking, M. J. J.; de Vivie-Riedle, R.; Kling, M. F. Attosecond Control of Electron Dynamics in Carbon Monoxide. *Phys. Rev. Lett.* **2009**, *103*, 103002.

(18) Bayer, T.; Braun, H.; Sarpe, C.; Siemering, R.; von den Hoff, P.; de Vivie-Riedle, R.; Baumert, T.; Wollenhaupt, M. Charge Oscillation Controlled Molecular Excitation. *Phys. Rev. Lett.* **2013**, *110*, 123003.

(19) Wollenhaupt, M.; Baumert, T. Ultrafast Strong Field Quantum Control on K_2 Dimers. *J. Photochem. Photobiol., A* **2006**, *180*, 248−255.

(20) Halász, G. J.; Perveaux, A.; Lasorne, B.; Robb, M. A.; Gatti, F.; Vibók, Á. Simulation Of Laser-induced Quantum Dynamics of the Electronic and Nuclear Motion in the Ozone Molecule on the Attosecond Time Scale. *Phys. Rev. A* **2012**, *86*, 043426−1−6.

(21) Halász, G. J.; Perveaux, A.; Lasorne, B.; Robb, M. A.; Gatti, F.; Vibók, Á. Coherence Revival During the Attosecond Electronic and Nuclear Quantum Photodynamics of the Ozone Molecule. *Phys. Rev. A* **2013**, *88*, 023425−1−6.

(22) Meyer, H.-D.; Manthe, U.; Cederbaum, L. S. The Multi-Configurational Time-Dependent Hartree Approach. *Chem. Phys. Lett.* **1990**, *165*, 73−78.

(23) Beck, M. H.; Jäckle, A.; Worth, G. A.; Meyer, H. D. The Multiconfiguration Time-Dependent Hartree (MCTDH) Method: A Highly Efficient Algorithm for Propagating Wavepackets. *Phys. Rep.* **2000**, *324*, 1−146. Worth, G. A.; et al. *The MCTDH Package*, Version 8.2, 2000; Version 8.3, 2002; Version 8.4, 2007; University of Heidelberg, Germany; see http://mctdh.uni-hd.de/.

(24) Perveaux, A.; Lauvergnat, D.; Lasorne, B.; Gatti, F.; Robb, M. A.; Halász, G. J.; Vibók, A. Attosecond Electronic and Nuclear Quantum Photodynamics of Ozone: Time-dependent Dyson Orbitals and Dipole. *J. Phys. B* **2014**, *47*, 124010.

(25) Wollenhaupt, M.; Engel, V.; Baumert, T. Femtosecond Laser Photoelectron Spectroscopy on Atoms and Small Molecules: Prototype Studies in Quantum Control. *Annu. Rev. Phys. Chem.* **2005**, *56*, 25−56.

(26) Stolow, A. Femtosecond Time-Resolved Photoelectron Spectroscopy of Polyatomic Molecules. *Annu. Rev. Phys. Chem.* **2003**, *54*, 89−119.

(27) Stolow, A.; Bragg, A. E.; Neumark, D. M. Femtosecond Time-Resolved Photoelectron Spectroscopy. *Chem. Rev.* **2004**, *104*, 1719−1757.

(28) Oana, C. M.; Krylov, A. I. Dyson Orbitals For Ionization from the Ground and Electronically Excited States Within Equation-of-Motion Coupled-cluster Formalism: Theory, Implementation, and Examples. *J. Chem. Phys.* **2007**, *127*, 234106−14.

(29) Oana, C. M.; Krylov, A. I. Cross Sections and Photoelectron Angular Distribution in Photodetachment from Negative Ions Using Equation-of-Motion Coupled-Cluster Dyson Orbitals. *J. Chem. Phys.* **2009**, *131*, 124114−15.

(30) Spanner, M.; Patchkovskii, S. One-Electron Ionization of Multielectron Systems in Strong Nonresonant Laser Fields. *Phys. Rev. A* **2009**, *80*, 063411−1−11.

(31) Spanner, M.; et al. Dyson Norms in XUV and Strong-field Ionization of Polyatomics: Cytosine and Uracil. *Phys. Rev. A* **2012**, *86*, 053406−1−9.

(32) Ohtsuka, Y.; Hasegawa, J.; Nakatsuji, H. Excited and Ionized States of Ozone Studied by the MEG (Multi-exponentially Generated)/EX (Excited)-MEG Method. *Chem. Phys.* **2007**, *332*, 262−270.
(33) Pickup, B. T. On the Theory of Fast Photoionization Process. *Chem. Phys.* **1977**, *19*, 193−208.
(34) Qu, Z. W.; Zhu, H.; Grebenshchikov, S. Y.; Schinke, R. The Photodissociation of Ozone in the Hartley Band: A Theoretical Analysis. *J. Chem. Phys.* **2005**, *123*, 074305−1−12.
(35) Grebenshchikov, S. Y.; Qu, Z. W.; Zhu, H.; Schinke, R. New Theoretical Investigations of the Photodissociation of Ozone in the Hartley, Huggins, Chappuis, and Wulf Bands. *Phys. Chem. Chem. Phys.* **2007**, *9*, 2044−2064.
(36) *MOLPRO*, version 2006,1, a package of ab initio programs, Werner, H.-J.; Knowles, P. J.; Lindth, R.; et al., see www.molpro.net.
(37) Knowles, P. J.; Werner, H. J. Internally Contracted Multi-configuration-Reference Configuration Interaction Calculations for Excited States. *Theor. Chim. Acta* **1992**, *84*, 95−103.